Experimental investigations on the correlations between the structure and thermal-electrochemical properties of over-discharged ternary/Si-C power batteries

Jiangyun Zhang[a, *], Xinxi Li[a,**], Guoqing Zhang[a], Hongwei Wu[b], Dan Shao[c], Xin Ge[a],

Qiqiu Huang [a], Zhicheng Zhen[a], Xuanzhuang Chen [a]

[a] School of Materials and Energy, Guangdong University of Technology, Guangzhou, Guangdong 510006, China

[b] School of Physics, Engineering and Computer Science, University of Hertfordshire, Hatfield, AL10 9AB, United Kingdom

[c] Guangdong Key Laboratory of Battery Safety, Guangzhou Institute of Energy testing, Guangzhou, Guangdong 511447, China

ABSTRACT

The thermal safety of power lithium-ion batteries（LIBs） has seriously affected the booming development of electric vehicles (EVs). Especially, owing to the requirement of high energy density, thermal runaway (TR) easily occurs in LIBs, resulting in a higher heat generation rate. Over-discharging is recognized as a common cause for TR. In the present research, the correlations between the structure and thermal-electrochemical properties of an over-discharged ternary/Si-C battery at

* Corresponding author.

** Corresponding author.

E-mail addresses: roseyyun@163.com (J. Zhang), pkdlxx@gdut.edu.cn (X. Li)

room and high temperatures were investigated. The heat generation mechanisms of the batteries due to the maximum surface temperature and peak temperature difference variations during fast charging and discharging processes were investigated. Moreover, the electrochemical performances parameters of the batteries, such as voltage changing trend, discharge time, discharge capacity, internal resistance, electrochemical impedance spectroscopy (EIS) spectra, were analyzed. When the battery was discharged at 2.0C and 55°C, its maximum temperature and highest temperature difference reached 91.34°C and 13.24°C, respectively, finally resulting in a sharp decline in electrochemical performance. Furthermore, the root reasons for performance degradation and heat generation intensification of the over-discharged battery (ODB) were analyzed by scanning electron microscopy (SEM) and X-ray diffraction (XRD). The cause of the aforementioned phenomenon is due to irreversible damage of the electrode materials. This research not only reveals the relevant relationship between the thermal behavior and the microscopic structure of the over-discharged ternary/Si-C battery under various temperature conditions but also provides valuable insights for improving the safety of LIBs modules even packs.

Keywords: Thermal safety, Over-discharge, Electrochemical performance, Heat generation, Ternary/Si-C power battery

Nomenclature			
Abbreviates			
EVs	Electric vehicles	NCM/C	$Li(Ni_{1/3}Co_{1/3}Mn_{1/3})O_2$/graphite
TR	Thermal runaway	BTMS	Battery thermal management system
EIS	Electrochemical impedance	ODB	Over-discharged battery

	spectroscopy		
SEM	Scanning electron microscope	NB	Normal battery
XRD	X-ray diffraction	SOCs	States of charge
LIBs	Lithium-ion batteries	R_p	Polarization resistance
BMS	Battery management system	R_{ct}	Charge transfer resistance
ISC	Internal short circuit	CC	Constant current
SEI	Solid electrolyte interface	CV	Constant voltage
SOH	State of health	A	Area (m^2)
C_p	Specific heat capacity ($kJ \cdot kg^{-1} \cdot K^{-1}$)	h	Heat transfer coefficient ($kW \cdot m^{-2} \cdot K^{-1}$)
m	Mass (Kg)	h_{eff}	Effective convective heat transfer coefficient ($W \cdot m^{-2} \cdot K^{-1}$)
q	Total heat (kJ)	T	Temperature （K）
T_0	Ambient temperature （K）	$\triangle T$	Temperature difference（K）
Greek letters			
ε	Emissivity	σ_r	Stefan–Boltzmann constant ($kW \cdot m^{-2} \cdot K^{-4}$)
ρ	Density, $kg \cdot m^{-3}$		
Subscripts			
b	Battery	c	Convection heat transfer
r	Radiation heat transfer	s	Stored in the battery
ct	Charge transfer	p	Polarization

1. Introduction

Lithium-ion batteries (LIBs) are one of the most promising power sources because of their high energy density and long service life [1−3]; thus, they are widely used in different engineering fields, ranging from portable electronics to electric vehicles (EVs) [4−6]. To meet the high-performance demand of EVs, ternary cathode and Si-C anode-based power batteries with relatively higher energy density have been developed. However, owing to the requirement of high energy density, the thermal

safety of integrated power systems is continuously aggravating, resulting in a thermal

runaway (TR) and even catastrophic accidents [7−9]. Unfortunately, the vulnerability

of the thermal sensitivity and thermal stability of a ternary cathode material would

aggravate TR due to the crystal structure of the material and the chemical reaction,

especially under overheating, overcharging, and over-discharging conditions [10, 11].

Over-discharging is mainly initiated by the failure of a battery management system

(BMS) and the inappropriate operation and performance inconsistency between

battery cells [12−14]. It is well known that over-discharging inevitably degrades the

electrochemical properties of a battery as the penetrated battery separator with the

unceasing growth of metallic dendrites generates an internal short circuit (ISC) [15,

16]. Therefore, it is important to investigate the fundamental thermal-electrochemical

properties and the correlation of the structure and performance of power batteries

under over-discharging conditions. Numerous studies have been conducted on the TR

mechanisms, failure mechanisms and models of power batteries under

over-discharging conditions [17−21]. During over-discharging, the anode potential of

a lithium-ion battery increases; thus, active substances on the Cu current collector are

oxidized to Cu^+ and Cu^{2+}. Moreover, the over-deintercalation of lithium ions

extracting from the anode is transferred to the cathode, resulting in the decomposition

of the solid electrolyte interface (SEI). Eventually, the battery separator becomes

damaged, causing an ISC during the over-discharging process [18, 19]. In addition,

the impacts of over-discharging on the electrochemical property degradations,

establishment of heat generation models, calculation of heat generation of power

batteries have been also investigated [22−24]. Ouyang et al. [25-27] analyzed the influences of over-discharging on the electro-thermal properties of power batteries with different chemical systems and noticed an increased declining rate of discharge capacity, internal resistance, energy density, and surface temperature due to over-discharging. Moreover, the electro-thermal parameters (temperature rise, capacity degradation rate) of the batteries increased exponentially with the rise of the over-discharge degree. Wang et al. [28] investigated the over-discharge behavior of a 2.9 Ah cylindrical $Li(Ni_{0.8}Co_{0.1}Mn_{0.1})O_2$/graphite battery under an adiabatic environment and asserted that a higher over-discharge rate resulted in a faster temperature rise. Broda et al. [29] conducted experiments to reveal the internal resistance and temperature changing trend during the over-discharging process of a lead-acid battery and found that the temperature and internal resistance of the battery increased remarkably under over-discharging conditions, manifesting severe influences on aging and capacity degradation. Qian et al. [30] investigated the cycle life decay behavior of a $Li(Ni_{1/3}Co_{1/3}Mn_{1/3})O_2$/graphite high-power battery during a slight over-discharging process and noticed a cycle life degradation of 15.4%. Moreover, the battery suffered from irreversible internal structure damage and phase transformation due to over-discharging. Zheng et al. [31] investigated the performance degradation and cycling stability of a $LiFePO_4$/C battery during an over-discharging process and reported that over-discharging led to serious irreversible loss of charging and discharging capacities. Moreover, the breakdown and dissolution of the SEI film resulted in severe electrochemical property degradation and poor

cycling performance. Erol et al. [32] analyzed the effects of over-discharging on the impedance response of a $LiCoO_2/C$ battery and noticed a reversibility of the impedance variation behavior of the over-discharged battery.

However, very few works have clarified the main reasons for internal crystalline structure destruction and performance degradation of anode and cathode electrode materials under over-discharging conditions, and it becomes the technical bottleneck of promoting the lifetime and thermal safety of batteries, especially for power battery packs with ternary/Si-C as the electrode material in EVs.

In the present research, the electrochemical performances of a ternary/Si-C battery, such as discharge voltage platform, discharge capacity and time, internal resistance, and electrochemical impedance spectroscopy (EIS) spectra, were analyzed. Moreover, the influences of temperature variations on the above-mentioned properties were also investigated. In addition, heat generation mechanisms during charging and discharging processes under room and high-temperature conditions were explored. Finally, the main reasons for electrochemical performance degradation and heat generation intensification were revealed. This illustration of the dependency between the interior structure destruction and the decreased electrochemical performance would be greatly benefited for the modification of electrode materials, thermal safety and the battery thermal management system (BTMS) designation.

2. Experiment

2.1 Governing equations

The electrochemical reaction of power LIBs is regarded as the disintercalation process of lithium ions. Lithium-ions can be inserted into or removed from the active material particles without affecting the original internal lattice structure of the electrodes. During the charging process, the lithium-ions are embedded from the positive electrode to the negative electrode. On the contrary, the lithium-ions are inserted from the negative electrode to the positive electrode during the discharge process. The entire electrochemical reaction process is considered to be reversible. Heat generation mechanism inside the battery is very complicated and is dependent on the electrochemical reaction rates. Heat production also changes with time and temperature. The x, y, z coordinates of battery heat flux can be described as follows based on the complex characteristics of the orthotropic materials during charging/discharging processes [33,34]:

$$q_x = -\lambda_{xx}\frac{\partial T}{\partial x} - \lambda_{xy}\frac{\partial T}{\partial y} - \lambda_{xz}\frac{\partial T}{\partial z} \quad (1)$$

$$q_y = -\lambda_{yx}\frac{\partial T}{\partial x} - \lambda_{yy}\frac{\partial T}{\partial y} - \lambda_{yz}\frac{\partial T}{\partial z} \quad (2)$$

$$q_z = -\lambda_{zx}\frac{\partial T}{\partial x} - \lambda_{zy}\frac{\partial T}{\partial y} - \lambda_{zz}\frac{\partial T}{\partial z} \quad (3)$$

The energy conservation equation of the battery cell is shown as follows:

$$\rho_b C_b \frac{\partial T_b}{\partial t} = \frac{\partial}{\partial x}\left(k_x \frac{\partial T_b}{\partial t}\right) + \frac{\partial}{\partial y}\left(k_y \frac{\partial T_b}{\partial y}\right) + \frac{\partial}{\partial z}\left(k_z \frac{\partial T_b}{\partial z}\right) + Q_b \quad (4)$$

Equation of conservation of mass is described as follows:

$$\frac{\partial u}{\partial x} + \frac{\partial v}{\partial y} = 0 \quad (5)$$

Equation of conservation of momentum is shown as follows:

$$\rho\left(u\frac{\partial u}{\partial x} + v\frac{\partial v}{\partial y}\right) = F_x - \frac{\partial P}{\partial x} + \mu\left(\frac{\partial^2 u}{\partial x^2} + \frac{\partial^2 u}{\partial y^2}\right) \qquad (6)$$

$$\rho\left(u\frac{\partial v}{\partial x} + v\frac{\partial u}{\partial y}\right) = F_y - \frac{\partial P}{\partial y} + \mu\left(\frac{\partial^2 v}{\partial x^2} + \frac{\partial^2 v}{\partial y^2}\right) \qquad (7)$$

Equation of conservation of energy is described as follows:

$$\rho C_p\left(u\frac{\partial T}{\partial x} + v\frac{\partial T}{\partial y}\right) = \lambda\left(\frac{\partial^2 T}{\partial x^2} + \frac{\partial^2 T}{\partial y^2}\right) \qquad (8)$$

As the processes of electrochemical reaction in the battery are very complex, it is very necessary to simplify the heat generation rate from the perspective of heat transfer. The total heat generation within the battery contains three parts and can be illustrated as follows:

$$q = q_s + q_c + q_r \qquad (9)$$

$$q_s = m_b C_p \frac{dT}{dt} \qquad (10)$$

$$q_c = h_{eff}A \Delta T \qquad (11)$$

$$q_r = \varepsilon\sigma_r A\left(T_b^4 - T_0^4\right) \qquad (12)$$

where q_s, q_c and q_r represent the heat stored in the battery, the heat transported to outer by convection heat transfer and radiation heat transfer, respectively.

2.2Preparation of power batteries

The technical parameters of an 18650-type ternary/Si-C power battery are presented in Table 1. Two batteries with excellent electrochemical performance consistency were selected. The first battery was charged under a 1.5C (the measurement of the charge and discharge current with respect to nominal capacity of the battery) constant-current (CC) charging mode with a cutoff voltage limit of 4.2 V and then again discharged under a constant-voltage (CV) charging mode until the cut-off current declined to 238 mA. After the charging experiment, the battery was

over-discharged at a rate of 2.0C until the cut-off voltage dropped to 2.0 V. The aforementioned charging-discharging procedures were repeated 100 times at room temperature (25°C) to obtain an over-discharged battery (ODB). After the over-discharging test, the internal resistance of ODB was raised by 12% from 40.51 mΩ to 45.38 mΩ. For comparison, the second battery was marked as a normal battery (NB) without conducting the aforesaid operations. The photos of NB and ODB are shown in Fig. 1.

Table 1 Technical parameters of an 18650-type ternary/Si-C power battery

Items	Technical parameters
Nominal voltage/capacity (V/Ah)	3.6/3.2
Cathode/Anode materials	$Li(Ni_{0.8}Co_{0.1}Mn_{0.1})O_2$ / Si-C
Electrolyte material	Carbonic ester
Cut-off voltage of charge (V)	4.2
Cut-off voltage of discharge (V)	2.75
Maximum charge rate (C)	1.5
Maximum discharge rate (C)	2.0
Standard charge rate (C)	0.2
Dimension (mm)	Diameter:18
	Height: 65
Weight (g)	39
Mass energy density (Wh/kg)	295.40
Volume energy density(Wh/L)	696.9

Fig. 1 Photos of NB and ODB

2.3 Experimental settings

The experimental system is schematically displayed in Fig. 2. A calorstat (BTH-80 C, Dongguan Bell Measuring Equipment Co. Ltd., China; Temperature range: -40−150°C) was used to maintain constant-temperature working conditions of 25°C and 55°C. NB and ODB were placed in the battery testing cabinet (CT-3001 W-50 V/120 A-NTF, Shenzhen Xinwei Co. Ltd., China) to conduct charging-discharging operations with an acquisition interval of one second. T-type thermocouples (OMEGA-type TT-T-30-SLE-1 M; Accuracy = ±0.1°C) were adhered to the positive, middle, and negative positions of NB and ODB (as shown in Fig. 3) to measure temperatures, and the original temperature data were recorded by a temperature patrol instrument (34901 A, Keysight Technology Co. Ltd., China) at an interval of one second during the electrochemical reaction process. An internal resistance meter (BK-300, Guangzhou Blue-Key electronic industry Co. Ltd., China) was used to detect the internal resistances of NB and ODB with different states of charge (SOCs). In addition, an electrochemical workstation (ZIVESP 1, Shanghai Anzinc Co. Ltd., China) was used to determine EIS spectra.
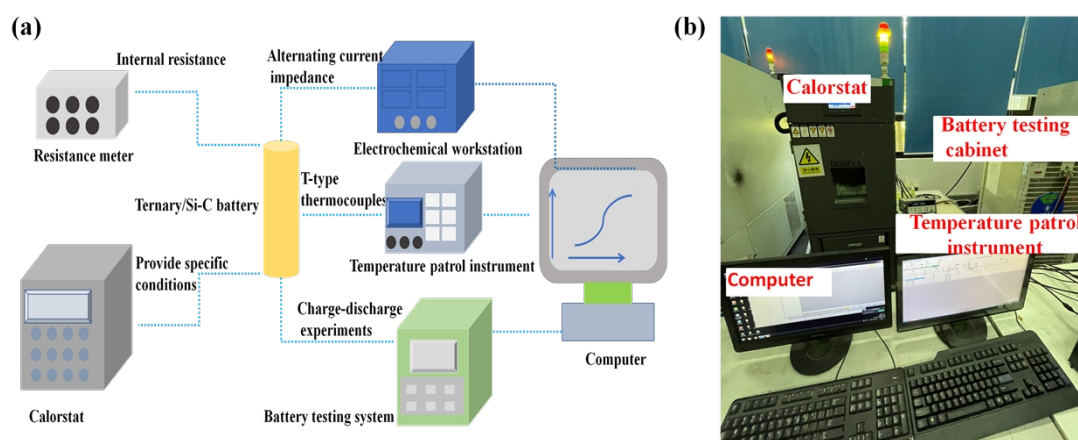
Fig. 2 Particular settings of the overdischarging experiments: (a) schematic diagram of the experimental platform and (b) actual experiment set-up
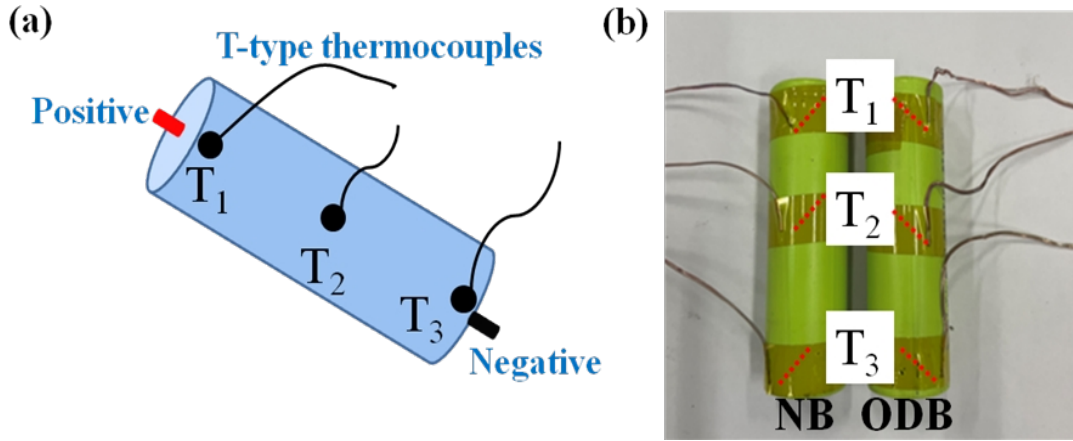
Fig. 3 Arrangement of T-type thermocouples: (a) particular schematic of the layout of the thermocouples and (b) actual diagrams of the placement of the thermocouples

2.4 Electrochemical property measurement

To analyze the influences of over-discharging on the electrochemical properties of ternary/Si-C power batteries at different temperatures and discharge currents, fully-charged NB and ODB were placed in the calorstat under constant-temperature conditions of 25°C and 55°C to perform discharging experiments at 0.5C, 1.0C, and 2.0C, and subsequently, the discharged capacity degradation, discharge time and voltage platform variation of ODB and NB were analyzed. The calculation method for discharge capacity is depicted in our previous work [35].

In addition, the internal resistances of NB and ODB with different SOCs ranging from 0% to 100% at 25°C and 55°C were evaluated. First, NB and ODB were charged in a galvanostatic mode at a rate of 1.5C with a voltage cut-off limit of 4.2 V and then charged in a potentiostatic mode until the charge current declined to 238 mA. Subsequently, the two fully charged batteries were discharged in a CC mode at 1.0C by taking 5% of the nominal capacity (3.2 Ah) as the discharge capacity interval point.

During the discharging process, discharge current and capacity were set as key experimental parameters to obtain the internal resistances of the batteries under different SOCs, which could refer to our previous work [35].

The EIS spectra of NB and ODB were measured by the electrochemical workstation at room temperature (25°C) with an alternating current amplitude voltage of 5 mV and a frequency range of 100000−0.001 Hz.

2.5 Heat generation analysis

The temperature variations of NB and ODB at 25°C and 55°C during the fast-charging process were compared. The charging rate of 1.5C was considered as the maximum value (Table 1). NB and ODB were first charged in a CC mode at 1.5C until the charge voltage reached 4.2 V and then charged in a constant-voltage mode until the charge current decreased to 238 mA. The charging experiment was conducted under a constant-temperature condition.

Moreover, to analyze the heat generation mechanism during the discharging process, discharging experiments of NB and ODB were conducted at 0.5C, 1.0C, and 2.0C rates under constant temperature conditions of 25°C and 55°C. The maximum temperatures and peak temperature differences between NB and ODB were measured and compared.

2.6 Microstructural characterization

2.6.1 Scanning electron microscope (SEM)

After the aforementioned experiments, NB and ODB (SOC = 0%) were placed

and dissected in a Mikrouka glove box under an argon atmosphere at 25°C, and the detailed process is displayed in Fig. 4. The purple insulating plastic film outside the battery was first peeled off, and the naked metal steel shell was then slowly stripped off by a tweezer. During this process, the caps of the positive and negative poles fell off first. Then the unique winding structure of the diaphragm, and anode and cathode electrode slices was clearly observed. To prevent a short circuit, the anode and cathode electrode slices with active substances attached were separated carefully. What was noticing was that short circuit should be prevented throughout the whole disassembly process. The obtained completed slices were carefully washed with dimethyl carbonate using the cotton swabs under the temperature condition of 25°C. Conductive powers were then gingerly extracted from the processed electrode slices using tool knife and dried in an oven (DHG-9070 A, Shanghai Jinghong Co. Ltd.) for 12 h at 80°C. Subsequently, active substances from the conductive pads were successfully extracted for further microscopic analyses by a SEM (Hitachi S-3400N-II, Japan) with an accelerating voltage of 20 kV.

| The intact commercial battery | Peel off the insulating film | Tear off the steel shell |

| Anode and cathode material | Electrode slices | Winding configuration |
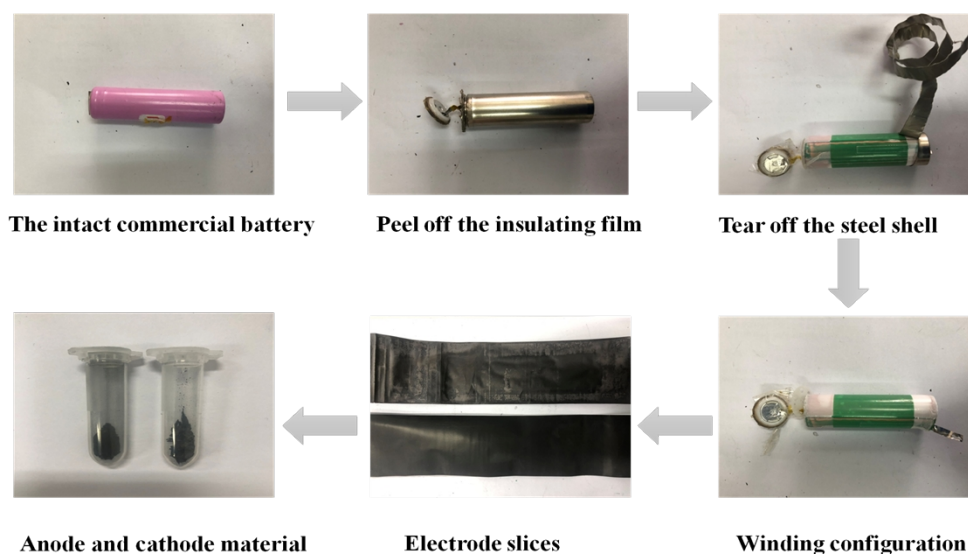
Fig. 4 Disassembly procedures of NB and ODB

2.6.2 X-ray diffraction (XRD) analysis

The crystal structures of active substances extracted from the anode and cathode electrodes slices were detected by a diffractometer (Rigaku D/max-2550) under Cu-Kα radiation (0.154056 nm) in the 2θ range of 10°−90° with a scanning speed of 6°·min⁻¹.

3. Results and discussion

3.1 Voltage platform and discharge capacity after over-discharging
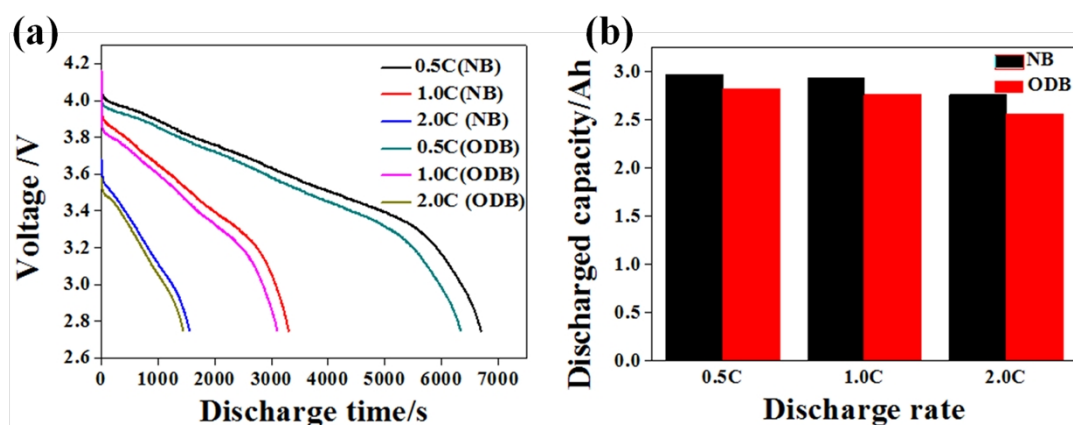
Fig. 5 Comparison of (a) discharge voltage platform and (b) capacity after over-discharging at 25°C

Table 2 Discharge times and capacities of NB and ODB at room temperature

	Discharge time (s)			Discharge capacity (Ah)		
	0.5C	1.0C	2.0C	0.5C	1.0C	2.0C
NB	6693	3301	1554	2.97	2.93	2.76
ODB	6336	3102	1441	2.82	2.76	2.56

Fig. 5 displays the fundamental electrochemical properties (discharge voltage

platform and capacity) of NB and ODB at different discharging currents under the room temperature condition of 25°C. It is noticeable from Fig. 5(a) that the discharge voltage and the rise of the voltage dropping rate declined with the increasing discharge rate during over-discharging; thus, shortening the discharge time and attenuating the discharge capacity (Fig. 5(b)). It is clear from Table 2 that the discharge times of ODB were 6336 s, 3102 s, and 1441 s at 0.5C, 1.0C, and 2.0C discharge rates, respectively, manifesting 5.63%, 6.42%, and 7.84% reductions as compared to those of NB, respectively. Moreover, the discharge capacities of ODB after over-discharging were 2.82 Ah, 2.76 Ah, and 2.56 Ah at 0.5C, 1.0C, and 2.0C discharge rates and these values are similar to those obtained by the equation of discharge capacity described in our previous work [35].
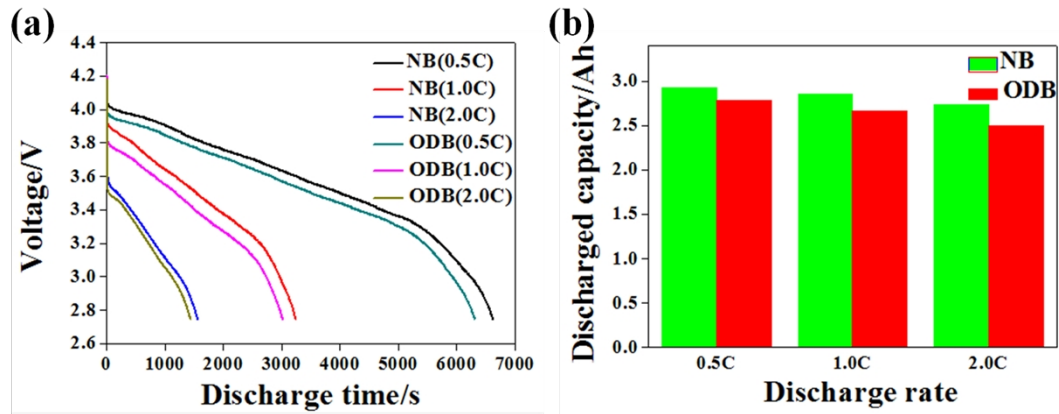
Fig. 6 Comparison of (a) discharge voltage platform and (b) capacity after over-discharging at 55°C

Table 3 Discharge times and capacities of NB and ODB at 55°C

	Discharge time (s)			Discharge capacity (Ah)		
	0.5C	1.0C	2.0C	0.5C	1.0C	2.0C
NB	6596	3221	1542	2.93	2.86	2.74

ODB	6286	3008	1407	2.79	2.67	2.50

To explore the influences of over-discharging on the electrochemical performance of power batteries at high temperatures, CC discharge experiments of NB and ODB were conducted at 55°C under 0.5C, 1.0C, and 2.0C discharge rates. The changes in the voltage platform and discharge capacity of NB and ODB are displayed in Figs. 6(a) and 6(b), respectively. It is clear that over-discharging caused a decrease of voltage platform, discharge time, and capacity and further aggravated electrochemical properties. It could be attributed to the ISC current caused by the movement of electrons from the anode to the cathode through copper deposition, resulting in a higher voltage-dropping rate. It is evident from Table 3 that the discharge capacities of ODB were 2.79 Ah, 2.67 Ah, and 2.50 Ah at 0.5C, 1.0C, and 2.0C, respectively, manifesting 5.02%, 7.12%, and 9.6% reductions as compared to those of NB, respectively. Moreover, when the discharge rate increased to 2.0C, the discharge capacity experienced a more severe decline due to the high-temperature condition. Therefore, the energy storage capacity degradation of ODB was exacerbated after over-discharging at the high temperature.

3.2 Internal resistance variation after over-discharging
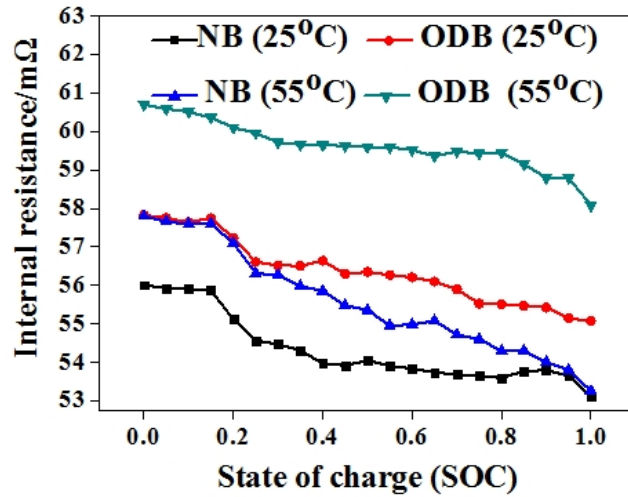
Fig. 7 Internal resistance variations of NB and ODB with different SOCs at 25°C and 55°C

The effects of over-discharging on ion/electron migration and electrolyte diffusion/transfer capability were analyzed by examining the internal resistances of NB and ODB and the Nyquist plots obtained from EIS tests. The internal resistance variations of NB and ODB with different SOCs at 25°C and 55°C are displayed in Fig. 7. It is noticeable that the internal resistance of ODB increased significantly after over-discharging at 25°C and 55°C. At the start (SOC = 100%) and end (SOC = 0%) of the CC discharge process at 55°C, the internal resistance of ODB increased by 9.05% and 5.02%, respectively.

3.3 EIS analysis of NB and ODB
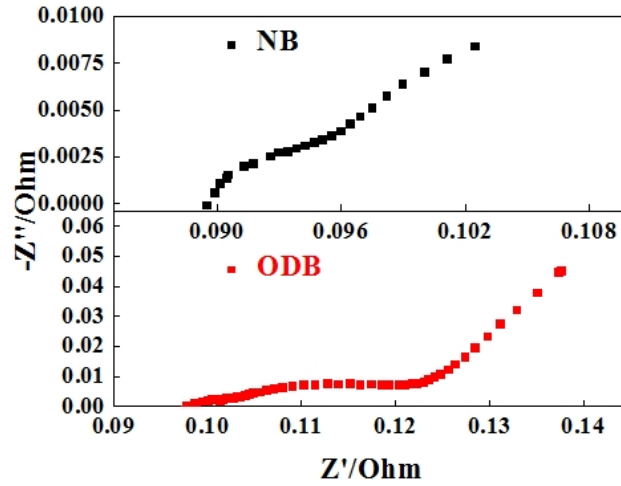
Fig. 8 Nyquist plots of NB and ODB with SOC = 0%

It is known that the equivalent series and polarization/charge transfer resistances (R_p/R_{ct}) of an electrode can be calculated from the initial intersection of curves and the semicircle diameter of a Nyquist plot, respectively. Fig. 8 compares the alternating-current impedance spectra of NB and ODB with 0% SOC at room temperature (25°C). In comparison to NB, ODB had much higher equivalent series (97.4 versus 89.4 mΩ) and R_p/R_{ct} (24.6 versus 6 mΩ) resistances after over-discharging. Therefore, the rise of electrical resistances aggravated the heat generation behavior of ODB.

3.4 Heat generation mechanism during the rapid charging process

18
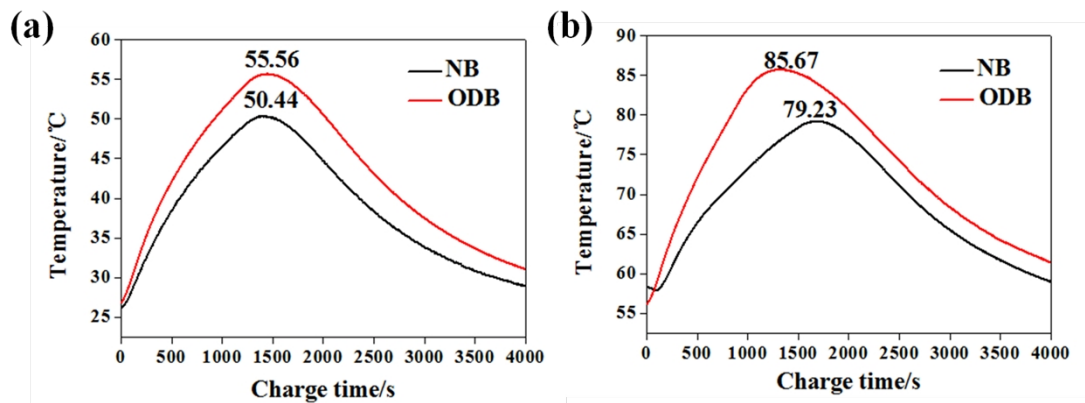
Fig. 9 Comparison of heat generation mechanisms of NB and ODB at 1.5C: (a) 25°C and (b) 55°C

To analyze the heat generation mechanisms of NB and ODB during the charging stage, charging experiments were conducted at 1.5C in CC/CV modes at 25°C and 55°C. The temperature changing curves of NB and ODB during the charging process are exhibited in Fig. 9. It is noticeable from Fig. 9(a) that the temperatures of NB and ODB gradually increased with the rise of the charging time before 1500 s during the CC charging stage. The maximum temperature of ODB reached 55.56°C (5.12°C higher than that of NB) with a steeper temperature rising slope at 25°C. In contrast, at 55°C, ODB achieved the maximum temperature of 85.67°C (6.44°C higher than that of NB) at 1275 s (Fig. 9(b)). It is worth noting that ODB attained the peak temperature earlier than NB with a higher temperature rising gradient at both 25°C and 55°C. The aforementioned result can be attributed to the damaged reversibility of active substances in positive and negative electrodes caused by overdischarge abuse. Hence, fast charging directly affects the operation safety of power batteries, shortens the service life, and makes the state of health (SOH) worse, and makes it more possible to cause TR after over-discharging. However, the temperature dropped slowly after reaching the peak value, and it could be attributed to the gradual decrease of the CC during the subsequent CV charging stage.

3.5 Heat generation mechanism during the discharging stage
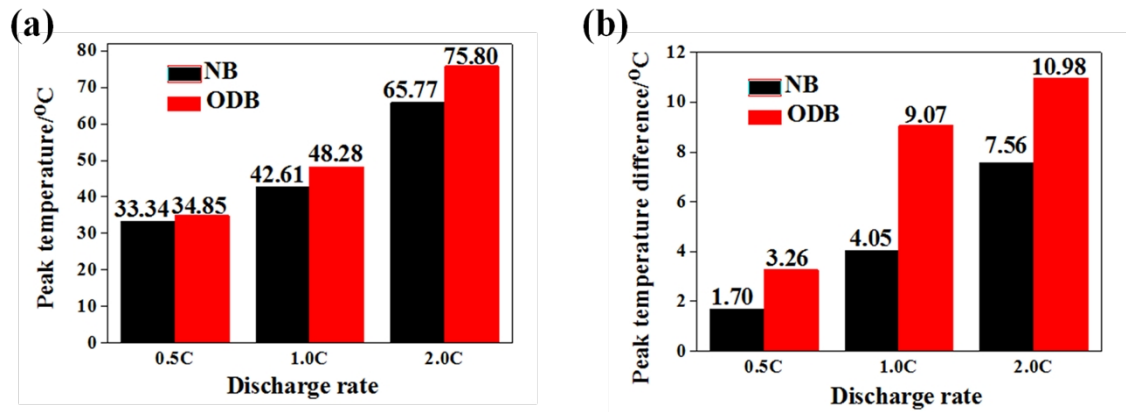
Fig. 10 Comparison of (a) peak temperature variations and (b) peak temperature difference changes of NB and ODB during the CC discharge process at 25°C

To further investigate the heat generation mechanisms of NB and ODB during the discharging process, constant-current discharging experiments were conducted at 25°C and 55 °C under 0.5C, 1.0C, and 2.0C. Fig. 10 compares the changes of the maximum temperature and temperature difference between NB and ODB during the CC discharge process. It is observable from Fig. 10(a) that the maximum temperature of ODB continued to rise with the increase of the discharge ratios and was always higher than that of NB at room temperature. Especially at 2.0C discharge rate, the maximum temperature of ODB reached 75.80°C, which was 15.3% higher than that of NB. Moreover, the temperature consistency of ODB and NB after over-discharging was aggravated continuously with the increase of the discharge ratio. It is clear from Fig. 10(b) that the peak temperature differences of ODB were 3.26°C, 9.07°C, and 10.98°C at 0.5C, 1.0C, and 2.0C discharge rates, respectively, manifesting 1.56°C, 5.02°C, and 3.42°C increments as compared to those of NB.

20
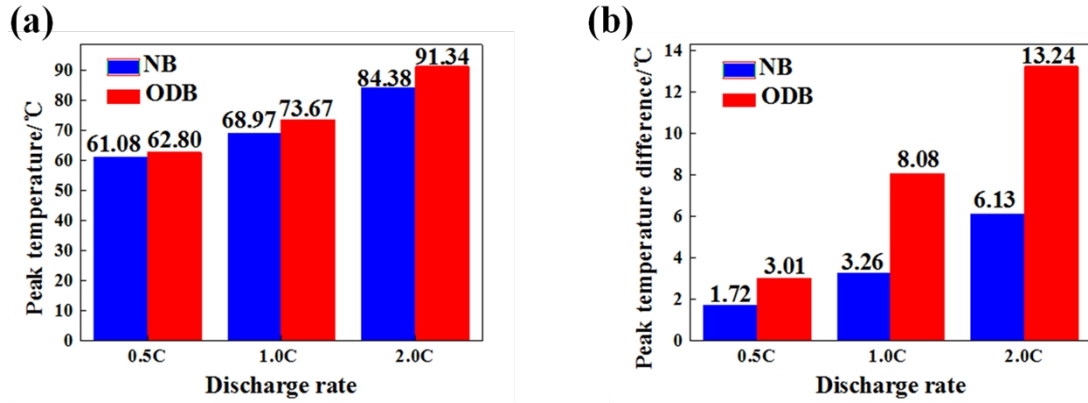
Fig. 11 Comparison of (a) peak temperature variations and (b) temperature consistency changes of NB and ODB during the discharging process at 55°C

Moreover, NB manifested a similar temperature variation law at 55°C. When the discharge ratio reached 2.0C, the peak temperature and maximum temperature difference of ODB after over-discharging were 91.34°C (Fig. 11(a)) and 13.24°C (Fig. 11(b)), respectively, which were 6.96°C and 7.11°C higher than those of NB, respectively. Therefore, the thermal behavior and temperature consistency of ODB were aggravated after over-discharging, causing a severe decline of electrochemical performance, the secondary destruction of the electrode material, which would make the battery more prone to TR.

Overall, from the aforementioned analysis data, we could draw a conclusion that the over-discharge, as the most common trigger for battery failure, inevitably led to the destruction of the internal structure of electrode materials, further hindering the normal embedding and extruding abilities of lithium ions, and eventually resulting in the serious deterioration of electrochemical performance and aggravation of heat generation behaviors. Hence, SEM and XRD micro-characterization tests of the electrode materials were conducted to analyze the essential reasons for the fading

performance.

3.6 XRD patterns of electrode materials
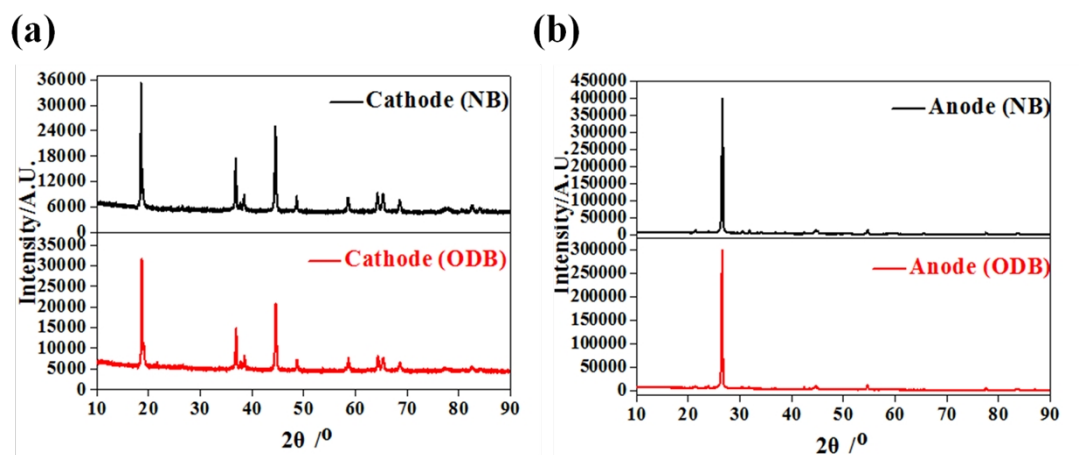
Fig. 12 XRD patterns of anode and cathode materials: (a) cathodes of NB and ODB and (b)

anodes of NB and ODB

Fig. 12 displays the internal crystal structural changes of electrode materials for

NB and ODB. The characteristic peaks of the cathode (NB and ODB) were located at

$2\theta = 18.67°, 36.95°, 38.60°, 44.57°, 48.68°, 58.54°, 64.09°, 65.53°, 68.60°, 82.59°$

(Fig. 12(a)), and those of the Si/C anode were located at $2\theta = 26.67°, 44.77°, 54.63°,$

$65.53°, 77.66°, 83.81°$ (Fig. 12(b)). Moreover, no impurity peaks were detected during

the over-discharging process. The peak values of both positive and negative electrode

materials were greatly reduced due to over-discharging, indicating that the

crystallinity of electrode substances decreased and the electrochemical performance

of ODB and NB seriously deteriorated.

3.7 SEM images of active substances
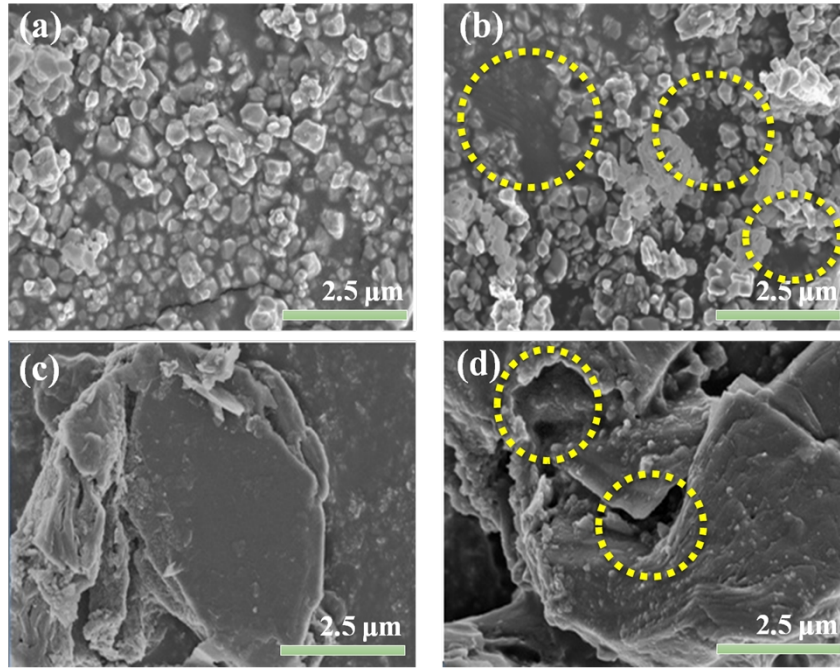
Fig. 13 Microstructures of electrode materials: (a) cathode of NB, (b) cathode of ODB, (c) anode of NB, and (d) anode of ODB

Fig. 13 exhibits the microstructures of positive and negative electrode materials of ODB and NB under normal and over-discharge conditions. A slight agglomeration of cathode electrode materials was noticed in ODB after over-discharging (Fig. 13(b)), whereas a dense arrangement of uniform particles accompanied by some interspaces between conductive substances was observed in NB (Fig. 13(a)). Moreover, in comparison to the smooth surface of conductive substances of NB anode slices (Fig. 13(c)), some loose gaps among anode materials and white silicon particles on the rough surface of graphite were detected in ODB after over-discharging (Fig. 13(d)). Therefore, the over-discharging of ODB destroyed the distribution of conductive particles and reduced the storage capacity.

3.8 Section morphology of electrode slices
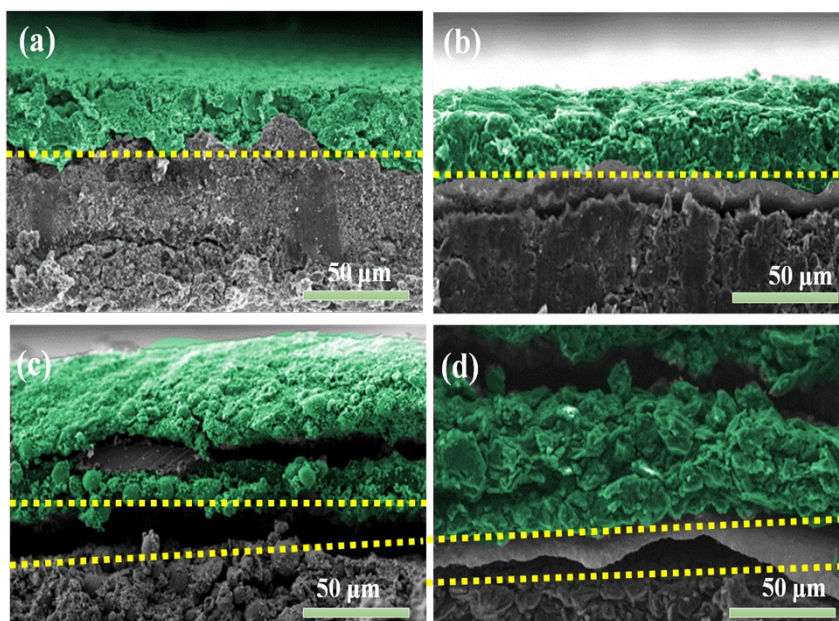
Fig. 14 SEM images of the cross-sections of electrode slices for NB and ODB: (a) cathode of NB, (b) anode of NB, (c) cathode of ODB, and (d) anode of ODB

Fig. 14 exhibits the SEM images of the cross-sections of electrode slices for NB and ODB. In comparison to a regular and compact distribution of active substances of cathode slices in NB (Fig. 14(a)), active substances of cathode slices in ODB were regularly distributed. Moreover, a serious peeling phenomenon on the cathode electrode plate occurred in ODB (Fig. 14(c)). For anode active materials, the above-mentioned phenomenon became worse. In comparison to the tight and neat distribution of anode materials in NB (Fig. 14(b)), anode substances appeared disorderly in ODB (Fig. 14(d)). Hence, the structure of active materials was seriously damaged, slowing down the embedding of lithium ions and the diffusion of the electrolyte. Consequently, the electrochemical performances of ODB seriously deteriorated.

4. Conclusions

The influences of over-discharging on the electrochemical properties and thermal behavior of a ternary/Si-C power battery were investigated. Additionally, the correlation between the performance deterioration and damaged internal structural was evaluated. The main inferences are summarized below.

(1)The voltage platform of the overdischarged ternary/Si-C battery dropped sharply, and this phenomenon got worse with the rise of the discharge rate. Moreover, the discharge time and capacity of the ternary/Si-C power battery were seriously attenuated at 55°C.

(2) The over-discharge of the ternary/Si-C power battery decreased the discharge time and capacity and also increased the internal resistance and impedance, leading to severely ascending heat generation and temperature inhomogeneity.

(3) The damage of the internal morphology and crystal structure of electrode materials were the fundamental reasons for electrochemical performance degradation and heat generation intensification, seriously hindering the normal electrochemical reaction and reducing the energy storage ability of the ternary/Si-C battery.

This study provides a research basis for the degradation mechanism of overdischarged ternary/Si-C cells. Moreover, the findings are beneficial to the optimization of electrode materials and the designation of thermal management systems.

References

[1] Liu JW, Li H, Li WY, et al. Thermal characteristics of power battery pack with liquid-based thermal management. Appl Therm Eng 2020;164:114421

[2] Wiriyasart S, Hommalee C, Sirikasemsuk S, et al. Thermal management system with nanofluids for electric vehicle battery cooling modules. Case Stud Therm Eng 2020;18:100583

[3] Shen M, Gao Q. System simulation on refrigerant-based battery thermal management technology for electric vehicles. Energ Convers Manage 2020;203:112176

[4] Liao ZH, Zhang S, Li K, et al. Hazard analysis of thermally abused lithium-ion batteries at different state of charges. J Energy Storage 2020;27:101065

[5] Srinivasan R, Thomas ME, Airola MB, et al. Preventing cell-to-cell propagation of thermal runaway in lithium-ion batteries. J. Electrochem. Soc 2020;167(2): 020559

[6] Tran MK, Bhatti A, Vrolyk R, et al. A review of range extenders in battery electric vehicles: current progress and future perspectives. World Electr. Veh. J. 2021;12(2):54.

[7] Feng XN, Ouyang MG, Liu X, et al. Thermal runaway mechanism of lithium ion battery for electric vehicles: A review. Energy Storage Mater 2018;10:246-267.

[8] Gandoman FH, Jaguemont J, Goutam S, et al. Concept of reliability and safety assessment of lithium-ion batteries in electric vehicles: basics, progress and challenges. Appl Energ 2019;251:113343

[9] Feng XN, Zheng SQ, Ren DS, et al. Investigating the thermal runaway mechanisms of lithium-ion batteries based on thermal analysis database. Appl Energ 2019;246:53-64

[10] Lai X, Zheng YJ, Zhou L, et al. Electrical behavior of overdischarge-induced internal short circuit in lithium-ion cells. Electrochim Acta 2018;278:245-254.

[11] Liao ZH, Zhang S, Li K, et al. A survey of methods for monitoring and detecting thermal runaway of lithium-ion batteries. J Power Sources 2019;436:226879

[12] Sidhu A, Izadian A, Anwar S. Adaptive nonlinear model-based fault diagnosis of li-ion batteries. IEEE T Ind Electron 2015;62(2);1002-1011.

[13] Carkhuff BG, Demirev PA, Srinivasan R. Impedance-based battery management system for safety monitoring of lithium-ion batteries. IEEE T Ind Electron 2018;65(8):6497-6504.

[14]Jiang ZY, Qu ZG, Zhang JF, et al. Rapid prediction method for thermal runaway propagation in battery pack based on lumped thermal resistance network and electric circuit analogy. Appl Energ 2020;268:115007.

[15] Zhang LW, Zhao P, Xu M, et al. Computational identification of the safety regime of Li-ion battery thermal runaway. Appl Energ 2020;261:114440.

[16] Weng JW, Yang XQ, Ouyang DX, et al. Comparative study on the transversal/lengthwise thermal failure propagation and heating position effect of

lithium-ion batteries. Appl Energ 2019;255:113761.

[17] Wu C, Zhu CB, Sun JL, et al. Fault mechanism study on Li-ion battery at over-discharge and its diagnosis approach. Electrical Sys Transp 2017;7(1):48-54.

[18] Guo R, Lu LG, Ouyang MG, et al. Mechanism of the entire overdischarge process and overdischarge-induced internal short circuit in lithium-ion batteries. Sci Rep 2016;6:30248.

[19] Hendricks CE, Mansour AN, Fuentevilla DA, et al. Copper dissolution in overdischarged lithium-ion cells: X-ray photoelectron spectroscopy and X-ray absorption fine structure analysis. J Electrochem Soc 2020;167(9):090501.

[20] Conner F, Daniel JR, Judith JJ, et al. Elucidating copper dissolution phenomenon in li-ion cells under overdischarge extremes. J Electrochem Soc 2018;165(9):1639-1647.

[21] Kasnatscheew J, Borner M, Streipert B, et al. Lithium ion battery cells under abusive discharge conditions: Electrode potential development and interactions between positive and negative electrode. J Power Sources 2017;362:278-282

[22] Panchal, S., Mathew, M., Fraser, et al. Electrochemical thermal modeling and experimental measurements of 18650 cylindrical lithium-ion battery during discharge cycle for an EV. Appl Therm Eng 2018;135:123-32.

[23] Akhoundzadeh MH, Panchal S, Samadani E, et al. Investigation and simulation of electric train utilizing hydrogen fuel cell and lithium-ion battery. Sustain Energy Techn 2021;46:101234.

[24] Mevawalla A, Panchal S, Tran MK, et al. One dimensional fast computational

partial differential model for heat transfer in lithium-ion batteries. J Energy Storage 2021;37:102471.

[25] Ouyang DX, Weng JW, Chen MY, et al. Experimental analysis on the degradation behavior of overdischarged lithium-ion battery combined with the effect of high-temperature environment. Int J Energy Res 2020;44(1):229-241.

[26] Ouyang DX, Weng JW, Chen MY, et al. Impacts of current rates on the degradation behaviors of lithium-Ion batteries under over-discharge conditions. J Electrochem Soc 2019;166:3432-3440.

[27] Ouyang DX, Wang J. Experimental analysis on lithium iron phosphate battery over-discharged to failure. IOP Conf. Ser.: Earth Environ. Sci 2019;257:012043.

[28] Wang D, Zheng LL, Li XC, et al. Effects of overdischarge rate on thermal runaway of NCM811 Li-ion batteries. Energies. 2020;13(15):3885.

[29] Broda B, Inzelt G. Internal resistance and temperature change during over-discharge of lead-acid battery. J Electrochem Sci Eng 2018;8 (2):129-139.

[30] Qian K, Li YY, He YB, et al. Abuse tolerance behavior of layered oxide-based Li-ion battery during overcharge and over-discharge. Rsc Adv 2016; 6(80):76897-76904.

[31] Zheng Y, Qian K, Luo D, et al. Influence of over-discharge on the lifetime and performance of $LiFePO_4$/graphite batteries. Rsc Adv 2016;6(36): 30474-30483.

[32] Erol S, Orazem ME, Muller RP. Influence of overcharge and over-discharge on the impedance response of $LiCoO_2$/C batteries. J Power Sources 2014;270:92-100.

[33] Wang ZY, Li XX, Zhang GQ, et al. Experimental study of a passive thermal

management system for three types of battery using copper foam saturated with phase change materials. Rsc Adv 2017, 7, 27441.

[34] Wang ZY, Li XX, Zhang GQ, et al. Thermal management investigation for lithium-ion battery module with different phase change materials. Rsc Adv 2017, 7, 42909.

[35] Zhang JY, Li XX, Zhang GQ, et al. Experimental investigation on the essential cause of the degrading performances for an overcharging ternary battery. Int J Energy Res 2020, 44(4), 3134-3147.